Chalcogenide Letters Vol. 15, No. 11, November 2018, p. 535 - 543

MECHANICAL AND STRAIN-TUNABLE ELECTRONIC PROPERTIES OF JANUS MoSSe NANOTUBES

Y. Z. WANG*, R. HUANG, B. L. GAO, G. HU, F. LIANG, Y. L. MA
Department of Applied Physics, Huaiyin Institute of Technology, Jiangsu, 223003, China

Using first-principles calculations, we systematically investigate the electronic and mechanical properties of the MoSSe nanotubes (NTs). It is found that the chirality and the different surface atoms rain influence on their electronic structures, Young's modulus and Poisson's ratios. Similar with MoS_2 ($MoSe_2$) NTs, zigzag SMoSe (S outside and Se inside of the NT) and SeMoS (Se outside and S inside of the NT) NTs are direct band gap semiconductors, and armchair SMoSe and SeMoS NTs are indirect band gap semiconductors. We also find the order of the band gap is $E_{g(SeMoS)} > E_{g(MoS2)} > E_{g(MoSe2)} > E_{g(SMoSe)}$ for the NTs with the same index *n*. Meanwhile, the band gap and the electron effective mass of the NTs can be effective modulated under the uniaxial strain, even there is a semiconductor-to-metal transition at the tensile stain of about 8% for (14, 0) SMoSe NT. The order of the Young's modulus is $Y_{MoS2} > Y_{SeMoS} > Y_{SMoSe} > Y_{MoSe2}$ for NTs with the same index *n*. Our results could help to design the nanoscale strain sensor and optoelectronic devices.

(Received September 2, 2018; Accepted November 3, 2018)

Keywords: MoSSe nanotube, Electronic structure, Young's modulus, First-principles calculation

1. Introduction

Since the synthesis of WS_2 NTs in 1992[1], one dimensional transition metal dichalcogenide (TMD) NTs have triggered extensive research interest, such as MoS_2 NTs[2-5], $MoSe_2$ NTs[6], WSe_2 NTs[7], $WS_{2(1-x)}Se_{2x}$ NTs[8], SnS_2 NTs[9], CrS_2 NTs[10], and so on. Because of their outstanding physical and chemical properties, the TMD NTs have many potential applications, such as, photo-emitting devices[11], catalysis[8], transistors[12], Li-ion batteries[13], solid lubricants[14], and so on.

Recently, the Lu[15] and Zhang[16] groups have successfully synthesized independently the monolayer (ML) Janus MoSSe by fully replacing the top-layer S (Se) atoms of MoS_2 ($MoSe_2$) ML with Se (S) atoms. As shown in Fig. 1(a), ML Janus MoSSe is sandwiched S-Mo-Se configuration, such structure breaks the out-of-plane symmetry, leading to vertical dipoles. Owing to the distinctive structure, outstanding physical and chemical properties of the Janus ML MoSSe, many potential applications have been investigated, such as, water-splitting photocatalyst[17,18],

* Corresponding author: wyzong126@126.com

piezoelectricity[19], catalysis[20,21], optoelectronic device[22], phonon transport[23], pyroelectricity[24], and so on. Motivated by the successful synthesis of Janus ML MoSSe in experiments, its one-dimensional (1D) nanostructure has been investigated as a promising 1D material for the next-generation nanoelectronic device. Wang et. al have studied the electronic and magnetic properties of zigzag MoSSe nanoribbon modulated by the strain and external electric filed[25]. Wu at. al have investigated the tuning the indirect-direct band gap transition in the $MoS_{2-x}Se_x$ armchair NT by diameter modulation[26]. Previous studies have proved that strain engineering is a simple and promising way to modulate the electronic properties of low dimensional nanomaterials, such as, MoS_2 NTs[27], MoS_2 nanoribbons[28], CrS_2 NTs[10], MoSSe ML[29], SiC ML[30], and so on. To the best of our knowledge, mechanical properties and strain effects on the electronic properties of the MoSSe NTs is still lack.

In this work, we systematically investigate the mechanical and strain tunable electronic properties of the MoSSe NTs. We observe the electronic properties, Young's modulus and Possion ratio of the MoSSe NTs are dependent on the chirality and the different surface atoms. The band gap and effective mass of electron of the MoSSe NTs can be modulated by the uniaxial strain.

2. Computational methods

All the calculations are performed using the Vienna ab initio simulation package (VASP) with the density functional theory (DFT) using projector-augmented-wave (PAW) potentials[31-33]. The exchange-correlation potential is described by the generalized gradient approximation (GGA) of the Perdew-Burke-Ernzerhof (PBE) parameterization[34]. A cutoff energy of 500 eV is applied for the plane wave expansion of the valence wave functions. A *k*-point mesh of 1×1×11 is used for Brillouin zone sampling of the NTs for the structural optimizations, and thirty *k* points are sampled for computing the band structure. All the structures are fully relaxed until the atomic force is less than 0.01 eV/Å, and the convergence thresholds of energy is set to 10^{-5} eV. To avoid interactions between adjacent images, the vacuum region is more than 15 Å.

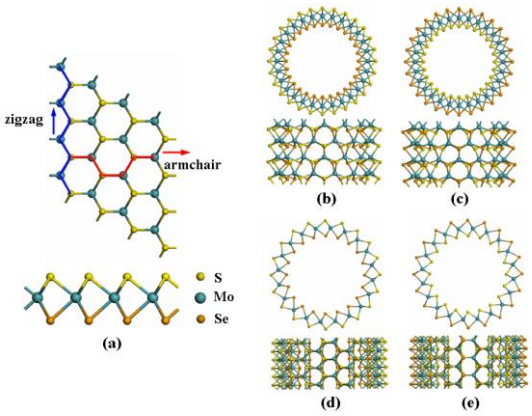

Fig. 1. The top and side view of the optimized structure of (a) MoSSe Janus monolayer, and (b) (14, 0) SMoSe, (c) (14, 0) SeMoS, (d) (10, 10) SMoSe and (e) (10, 10) SeMoS Janus nanotubes. The arrows indicate the rolling direction.

3. Results and discussion

At first, we optimize the geometry of ML Janus MoSSe, as shown in Fig. 1(a). The optimized lattice constant is a=b=3.25 Å, which is consistent with the previous results [23]. Similar to the carbon NTs, we can obtain the MoSSe NTs by rolling the MoSSe ML. Based on the zigzag and armchair rolling directions of the ML MoSSe, as shown in Fig. 1(a), the well-known zigzag for (n, 0) and armchair (n, n) NTs can be achieved. Besides, according to the different atoms of outer surface of the MoSSe NT, we also can obtain two different NTs for the same index n. For convenience, we name the MoSSe NT with the S outside as SMoSe NT, similarly, the MoSSe NT with the Se outside is named SeMoS NT. Fig. 1(b), (c), (d), (e) show the top and side view of the (14, 0) SMoSe, (14, 0) SeMoS, (10, 10) SMoSe, and (10, 10) SeMoS NTs. The optimized lattice constant and the radius of the NTs are shown in Table 1. For the (14, 0) SMoSe (SeMoS) NT, the lattice constant is 5.54 (5.52) Å, which is smaller than the value of 5.63 Å for the zigzag direction of MoSSe ML. On the contrary, the lattice constant of (10, 10) SMoSe (SeMoS) NT is slightly stretched with the value of 3.27 Å, compared to that of 3.25 Å for MoSSe ML.

Table 1. The calculated lattice constant (L_0), tube radius (R_0), Poisson ratio (υ) and Young's modulus (Y) of SMoSe and SeMoS Janus nanotubes, together with the MoS_2 and $MoSe_2$ nanotubes for comparison.

System	L_0 (Å)	R_0 (Å)	υ	Y (GPa)
MoS_2 (14, 0)	5.42	7.618	0.319	159.7
$MoSe_2$ (14, 0)	5.63	8.078	0.337	124.6
SMoSe (14, 0)	5.54	7.914	0.310	139.4
SeMoS (14, 0)	5.52	7.782	0.344	148.3
MoS_2 (10, 10)	3.20	9.083	0.317	175.7
$MoSe_2$ (10, 10)	3.34	9.576	0.318	145.0
SMoSe (10, 10)	3.27	9.413	0.333	153.4
SeMoS (10, 10)	3.27	9.236	0.304	165.4

As one of the important characterizations of mechanical properties of the NTs for practical applications of nanodevices, Young's modulus Y is defined as the second derivative of the total energy E with respect to the strain $\varepsilon_{\square}$ at the equilibrium volume V_0 by the following equation[27]:

$$Y = \frac{1}{V_0} \times \frac{\partial^2 E}{\partial \varepsilon_{\parallel}^2} = \frac{1}{2\pi R_0 L_0 \delta} \times \frac{\partial^2 E}{\partial \varepsilon_{\parallel}^2}$$

where R_0 and L_0 are the radius and the lattice constant of the unstrained NTs, δ indicates the thickness of the tube wall. In order to obtain the Young's modulus, the stain energies are calculated in the uniaxial strain range of -1% to 1%. For comparison, we also calculate the Young's modulus of MoS_2 and $MoSe_2$ NTs, as shown in Table 1. The Young's modulus of (14, 0) and (10, 10) MoS_2

NTs are 159.7 GPa and 175.7 GPa, respectively, which can be compared with those reported by Ansari et al.[35]. The Young's modulus of (14, 0) and (10, 10) SeMoS NTs are larger than that of (14, 0) and (10, 10) SMoSe NTs, respectively. We also find the order of the Young's modulus of the (14, 0) and (10, 10) NTs is $Y_{MoS2} > Y_{SeMoS} > Y_{SMoSe} > Y_{MoSe2}$, which is identical to that of the MoS_2, MoSSe, and $MoSe_2$ ML (MoS_2 > MoSSe > $MoSe_2$)[23].

We also calculate the Poisson ratio of the NTs, which can be obtained using the ratio of transverse contraction and axial elongation:

$$\nu = \frac{\varepsilon_{\perp}}{\varepsilon_{\square}} = -\frac{L_0}{R_0} \times \frac{\partial R}{\partial L}$$

where $\varepsilon_{\square}$ is the externally imposed strain along the tube axial direction, and $\varepsilon_{\perp}$ is the radial contraction strain. In table 1, the Poisson ratio of (14, 0) SeMoS NT is larger than that of (14, 0) SMoSe NT, on the contrary, the Poisson ratio of (10, 10) SeMoS NT is smaller than that of (10, 10) SMoSe NT. Which is due to the different topologies of the Mo-S and Mo-Se bonds of different orientation for zigzag (14, 0) and armchair (10, 10) NTs, as shown in Fig. 1. Comparing to the MoS_2 and $MoSe_2$ NTs, we also find the order of Poisson ratio for (14, 0) NTs is $\acute{\imath}_{SeMoS} > \acute{\imath}_{MoSe2} > \acute{\imath}_{MoS2} > \acute{\imath}_{SMoSe}$, while, for the (10, 10) NTs, which is $\acute{\imath}_{SMoSe} > \acute{\imath}_{MoSe2} > \acute{\imath}_{MoS2} > \acute{\imath}_{SeMoS}$. The above Young's modulus and Poisson ratio analysis results indicate the different surface atoms of MoSSe NTs will obviously affect their mechanical properties.

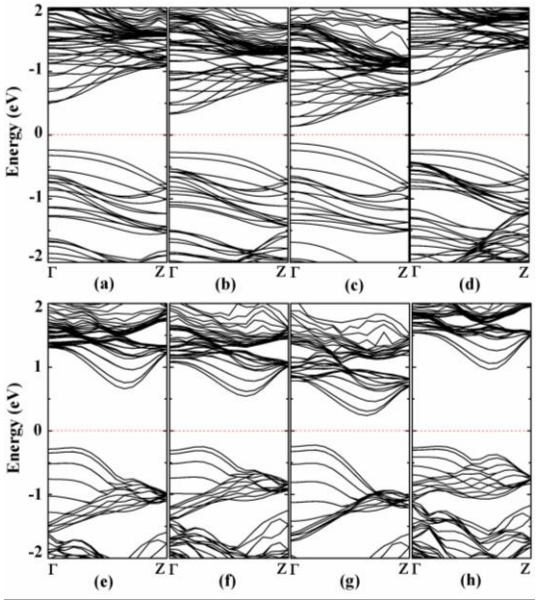

Fig. 2. Band structure of the zigzag (14, 0) (a) MoS_2, (b) $MoSe_2$, (c) SMoSe and (d) SeMoS nanotubes, and armchair (10, 10) (e) MoS_2, (f) $MoSe_2$, (g) SMoSe and (h) SeMoS nanotubes.

Fig. 2 shows the band structures of the (14, 0) and (10, 10) SMoSe, SeMoS, MoS_2 and $MoSe_2$ NTs without the uniaxial strain. The (14, 0) SMoSe and SeMoS NTs exhibit direct band gap with the valence band maximu (VBM) and conduction band minimum (CBM) at $\tilde{A}$-point,

while (10, 10) SMoSe and SeMoS NTs are indirect band gap semiconductors, which are similar with MoS_2 and $MoSe_2$ NTs. Interestingly, we find the band gap of (14, 0) SMoSe (E_g=0.268 eV) and (10, 10) SMoSe (E_g=0.465 eV) NTs are obviously smaller than that of (14, 0) SeMoS (E_g=1.019 eV) and (10, 10) SeMoS (E_g=1.207 eV) NTs, respectively. Comparing with MoS_2 and $MoSe_2$ NTs, the order of the band gap is $E_{g(SeMoS)} > E_{g(MoS2)} > E_{g(MoSe2)} > E_{g(SMoSe)}$ for (14, 0) and (10, 10) NTs, respectively. So the band gap of MoS_2 ($MoSe_2$) NT can be modulated by replacing the surface atoms of the NTs using the similar method to synthesize the MoSSe ML.

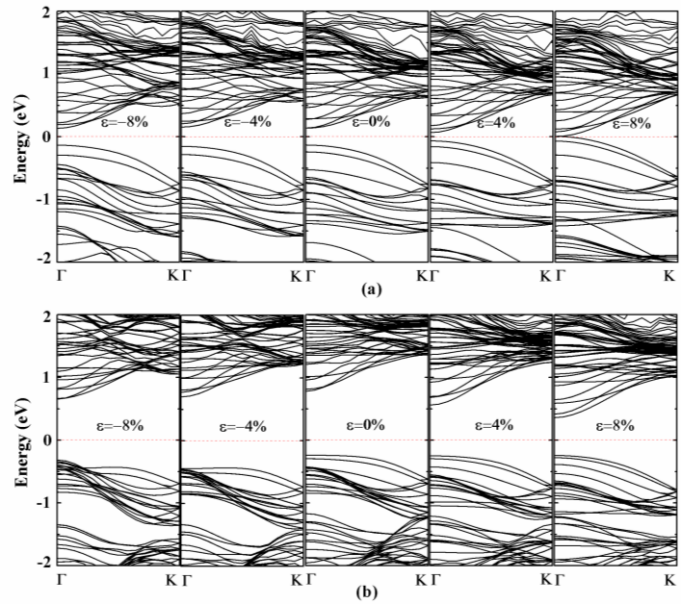

Fig. 3. Band structures of (a) (14, 0) SMoSe and (b) (14, 0) SeMoS nanotubes under uniaxial strain, respectively.

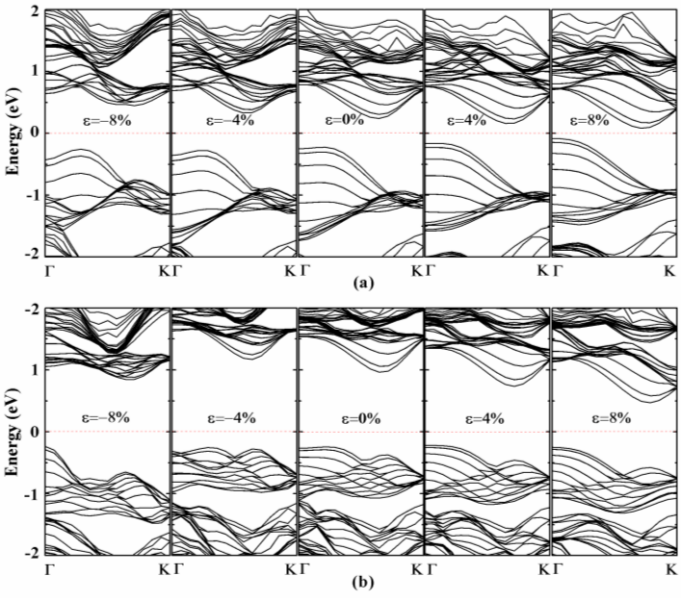

Fig. 4. Band structures of (a) (10, 10) SMoSe and (10, 10) SeMoS nanotubes under uniaxial strain, respectively.

The effects of strain on the band structures of the zigzag and armchair SMoSe (SeMoS) NTs have been investigated. Fig. 3 and Fig. 4 illustrate the band structures of the (14, 0) and (10, 10) SMoSe (SeMoS) NTs under uniaxial strain, respectively. We can see the compressive (tensile) strain can increase (reduce) the band gap for the zigag and armchair SMoSe (SeMoS) NTs. For (14, 0) SMoSe and SeMoS NTs, the VBM and CBM will maintain at $\tilde{A}$ under uniaxial strain. While, for (10, 10) SMoSe (SeMoS) NTs, the moving of the VBM occurs, but which are still indirect band gap. Interestingly, there is a semiconductor-to-metal transition at the tensile stain of about 8% for (14, 0) SMoSe NT. In contrast, for (14, 0) SeMoS and (10, 10) SMoSe (SeMoS) NTs, the band gap does not vanish up to 8% tensile strain.

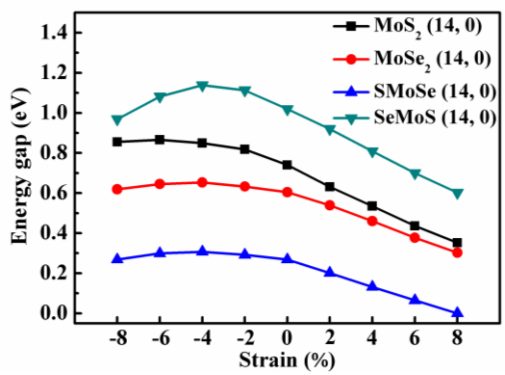

Fig. 5. Energy gap of (14, 0) SMoSe, SeMoS, MoS_2 and $MoSe_2$ nanotubes as a function of uniaxial strain.

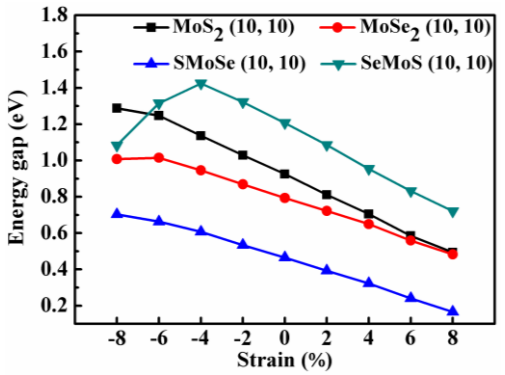

Fig. 6. Energy gap of (10, 10) SMoSe, SeMoS, MoS_2 and $MoSe_2$ nanotubes as a function of uniaxial strain.

Fig. 5 and Fig. 6 show the variations of the band gap of the zigzag and armchair NTs under the uniaxial strain. For the (14, 0) SMoSe and SeMoS NTs, the band gap decrease linearly under uniaxial tensile strain, while the band gap increase at first then decrease under uniaxial compressive strain. For the (10, 10) SMoSe NT, the band gap almost decrease linearly under the strain from -8% to 8%. However, for the (10, 10) SeMoS NT, the band gap decrease linearly under the strain from -4% to 8%, while the band gap decrease under the compressive strain from -4% to -8%. The variation trend of the band gap for the zigzag and armchair SMoSe (SeMoS) NTs is similar to that of the MoS_2 ($MoSe_2$) NTs.

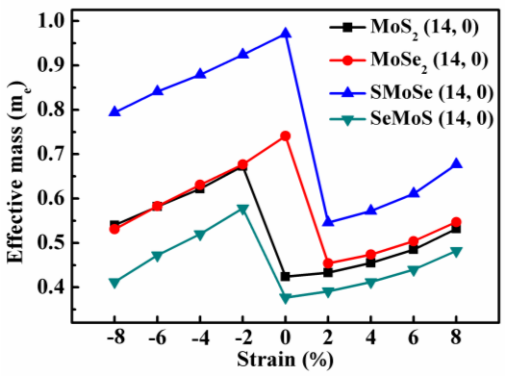

Fig. 7. The effective mass (in unites of the free electron mass m_e) of electron for (14, 0) SMoSe, SeMoS, MoS_2 and $MoSe_2$ nanotubes under uniaxial strain.

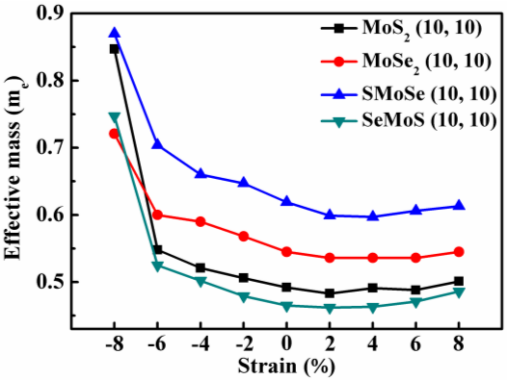

Fig. 8. The effective mass (in unites of the free electron mass m_e) of electron for (10, 10) SMoSe, SeMoS, MoS_2 and $MoSe_2$ nanotubes under uniaxial strain.

As shown in Fig. 3 and Fig. 4, the unaxial strain can change the band structures of the NTs, which is supposed to change the effective mass of electron. It can be calculated using the formula $m^* = \hbar^2 \left[d^2E(k)/dk^2 \right]^{-1}$ from the band structures, where *E(k)* is the energy band, *k* is the coordinate vector in the reciprocal space, and $\hbar$ is the reduced Planck constant. Fig. 7 and Fig. 8 show the effective mass of electron for the zigzag and armchair NTs under unaxial strain. Without strain, the effective mass of electron are 0.97, 0.38, 0.62 and 0.47 m_e for (14, 0) SMoSe, (14, 0) SeMoS, (10, 10) SMoSe and (10, 10) SeMoS NTs, respectively. It is obviously the effective mass of electron of SMoSe NT is larger than that of SeMoS NT without strain for the NT with the same index *n*. Comparing to MoS_2 and $MoSe_2$ NTs, the order of the effective mass of electron is $m_{e(SMoSe)} > m_{e(MoSe2)} > m_{e(MoS2)} > m_{e(SeMoS)}$ for (14, 0) and (10, 10) NTs under zero strain. For (14, 0) NTs, the effective mass of electron is sensitive to both compressive and tensile strain. The variation trend is similar with the (14, 0) CrS_2 NTs[10]. In contrast, for the (10, 10) NTs, the effective mass of electron is not sensitive to the tensile strain, while which increase with increasing the compressive strain.

4. Conclusions

In summary, the mechanical properties and the strain effects on the electronic properties of MoSSe NTs are systematically investigated. It is found that the Young's modulus of SeMoS NT is larger than that of SMoSe NT for the NT with the same index *n*. Similar with MoS_2 ($MoSe_2$) NTs, zigzag SMoSe and SeMoS NTs are direct band gap, and armchair SMoSe and SeMoS NTs possess indirect band gap. Interestingly, the band gap of SeMoS NT is obviously larger than that of SMoSe NT for the NT with the same index *n.*

Meanwhile, the band gap and the electron effective mass of the NTs can be effective modulated under the uniaxial strain, even there is a semiconductor-to-metal transition at the tensile stain of about 8% for (14, 0) SMoSe NT. Our results provide the fundamental insights of the MoSSe NTs, and pave the way for the potential applications of MoSSe NTs in optoelectronic devices and strain sensor.

Acknowledgements

This work was supported by the Foundation for the National Natural Science Foundation of China (11604113) and the Natural Science Foundation of the Jiangsu Higher Education Institutions of China (Grant No. 17KJB140004).

References

[1] R. Tenne, L. Margulis, M. Genut, G. Hodes, Nature **360**, 444 (1992).
[2] Q. L. Xiong, J. Zhang, C. Xiao, Z. H. Li, Phys. Chem. Chem. Phys. **19**, 19948 (2017).
[3] S. Li, W. Qi, S. Xiong, D. Yu, Appl. Phys. A **124**, 218 (2018).
[4] R. F. Cao, B. Zhou, C. F. Jia, X. D. Zhang, Z. Y. Jiang, J. Phys. D: Appl. Phys. **49**, 045106 (2016).
[5] Y. Z. Wang, B. L. Wang, Q. F. Zhang, R. Huang, B. L. Gao, F. J. Kong, X. Q. Wang, Chalcogenide Lett. **11**, 493 (2014).
[6] X. Wang, B. Zheng, B. Yu, B. Wang, W. Hou, W. Zhang, Y. Chen, J. Mater. Chem. A **6**, 7842 (2018).
[7] Z. Z. Yu, J. Wang, Phys. Rev. B **91**, 205431 (2015).
[8] K. Xu, F. M. Wang, Z. X. Wang, X. Y. Zhan, Q. S. Wang, Z. Z. Cheng, M. Safdar, J. He, ACS Nano **8**, 8468 (2014).
[9] Y. C. Huang, C. Y. Ling, X. Chen, D. M. Zhou, S. F. Wang, RSC Adv. **5**, 32505 (2015).
[10] Y. Z. Wang, R. Huang, X. Q. Wang, Q. F. Zhang, B. L. Gao, L. Zhou, G. Hu, Chalcogenide Letters **13**, 301 (2016).
[11] J. P. Mathew, G. Jegannathan, S. Grover, P. D. Dongare, R. D. Bapat, B. A. Chalke, S. C. Purandare, M. M. Deshmukh, Appl. Phys. Lett. **105**, 223502 (2014).
[12] M. Strojnik, A. Kovic, A. Mrzel, J. Buh, J. Strle, D. Mihailovic, AIP Adv. **4**, 097114 (2014).
[13] G. D. Li, X. Y. Zeng, T. D. Zhang, W. Y. Ma, W. P. Li, M. Wang, Cryst. Eng. Comm. **16**, 10754 (2014).

[14] J. Jelenc, M. Remskar, Nanoscale Res. Lett. **7**, 208 (2012).
[15] A. Y. Lu, H. Zhu, J. Xiao, C. P. Chuu, Y. Han, M. H. Chiu, C. C. Cheng, C. W. Yang, K. H. Wei, Y. Yang, Y. Wang, D. Sokaras, D. Nordlund, P. Yang, D. A. Muller, M. Y. Chou, X. Zhang, L. J. Li, Nat. Nanotech. **12**, 744 (2017).
[16] J. Zhang, S. Jia, I. Kholmanov, L. Dong, D. Q. Er, W. B. Chen, H. Guo, Z. H Jin, V. B. Shenoy, L. Shi, J. Lou, ACS Nano **11**, 8192 (2017).
[17] X. C. Ma, X. Wu, H. D. Wang, Y. C. Wang, J. Mater. Chem. A **6**, 2295 (2018).
[18] Y. J. Ji, M. Y. Yang, H. P. Lin, T. J. Hou, L. Wang, Y. Y. Li, S. T. Lee, J. Phys. Chem. C **122**, 3123 (2018).
[19] L. Dong, J. Lou, V. B. Shenoy, ACS Nano **11**, 8242 (2017).
[20] W. Z. Chen, Y. J. Qu, L. M. Yao, X. H. Hou, X. Q. Shi, H. Pan, J. Mater. Chem. A **6**, 8021 (2018).
[21] D. Q. Er, H. Ye, N. C. Frey, H. Kumar, J. Lou, V. B. Shenoy, Nano Lett. **18**, 3943 (2018).
[22] Y. Liang, J. W. Li, H. Jin, B. B. Huang, Y. Dai, J. Phys. Chem. Lett. **9**, 2797 (2018).
[23] S. D. Guo, Phys. Chem. Chem. Phys. **20**, 7236 (2018).
[24] J. Liu, S. T. Pantelides, Phys. Rev. Lett. **120**, 207602 (2018).
[25] M. Wang, Y. Pang, D. Y. Liu, S. H. Zheng, Q. L. Song, Comp. Mater. Sci. **146**, 240 (2018).
[26] H. H. Wu, Q. Q. Meng, H. Huang, C. T. Liu, X. L. Wang, Phys. Chem. Chem. Phys. **20**, 3608 (2018).
[27] W. F. Li, G. Zhang, M. Guo, Y. W. Zhang, Nano Res. **7**, 518 (2014).
[28] H. Pan, Y. W. Zhang, J. Phys. Chem. C **116**, 11752 (2012).
[29] M. Meng, T. H. Li, S. F. Li, K. L. Liu, J. Phys. D: Appl. Phys. **51**, 105004 (2018).
[30] L. B. Drissi, K. Sadki, M. H. Kourra, M. Bousmina, J. Appl. Phys. **123**, 185106 (2018).
[31] P. E. Blöchl, Phys. Rev. B **50**, 17953 (1994).
[32] G. Kresse, J. Furthmüller, Comp. Mater. Sci. **6**, 15 (1996).
[33] G. Kresse, J. Furthmüller, Phys. Rev. B **54**, 11169 (1996).
[34] J.P. Perdew, K. Burke, M. Ernzerhof, Phys. Rev. Lett. **77**, 3865 (1996).
[35] R. Ansari, S. Malakpour, M. Faghihnasiri, S. Sahmani, Superlattices Microst. **82**, 188 (2015).